Scalable Coupled Ocean and Water Turbine Modeling for Assessing Ocean Energy Extraction

Stefano Deluca*, Stefania Zanforlin*, Benedetto Rocchio†, Patrick J. Haley Jr.‡, Corbin Foucart‡, Chris Mirabito‡, Pierre F. J. Lermusiaux‡§

*Department of Energy, Systems, Territory and Constructions Engineering, University of Pisa, Largo Lucio Lazzarino, Pisa (PI) 56122, Italy
†Department of Civil and Industrial Engineering, University of Pisa, Largo Lucio Lazzarino , Pisa (PI) 56122, Italy
‡Department of Mechanical Engineering, Massachusetts Institute of Technology, 77 Massachusetts Avenue, Cambridge, MA 02139
§Corresponding author: pierrel@mit.edu

***Abstract*—The interest in hydrokinetic conversion systems has significantly grown over the last decade with a special focus on cross-flow systems, generally known as Vertical Axis Water Turbines (VAWTs). However, analyzing of regions of interest for tidal energy extraction and outlining optimal rotor geometry is currently very computationally expensive via conventional 3D Computational Fluid Dynamics (CFD) methods. In this work, a VAWT load prediction routine developed at University of Pisa based upon the Blade Element-Momentum (BEM) theory is presented and validated against high-resolution 2D CFD simulations. Our model is able to work in two configurations, i.e. Double-Multiple Streamtube (DMST) mode, using 1D flow simplifications for quick analyses, and Hybrid mode, coupled to a CFD software for more accurate results. As a practical application, our routine is employed for a site assessment analysis of the Cape Cod area to quickly highlight oceanic regions with high hydrokinetic potential, where further higher-order and more computationally expensive CFD analyses can be performed. Ocean data are obtained from data-assimilative ocean simulations predicted by the 4D regional ocean modeling system of the Multidisciplinary Simulation, Estimation, and Assimilation Systems (MSEAS) group of the Massachusetts Institute of Technology.**

I. Introduction

In the near future, exploiting tidal current energy could become an economically and technically feasible way of producing renewable energy and meeting our sustainability targets. Horizontal axis or cross-flow turbines, also known as Vertical Axis Water Turbines (VAWTs), can be used. The advantages of VAWTs are their cost-effectiveness, construction simplicity, and the ability to work independently of flow direction. Moreover, by adopting floating platforms, the generator and gearbox could be placed above the sea level, and it would be possible to harvest significantly higher energy from currents compared to devices fixed close to the sea bottom. Despite VAWTs exhibiting slightly lower efficiencies, this disadvantage is compensated by a higher packing factor in farms due to the much quicker wake dissipation [10, 12]. A further increase in energy production could be achieved by counter-rotating VAWTs placed in close proximity, which appear to have a mutually beneficial effect [29, 32, 31].

To assess the hydrokinetic potential of an area of interest a 4D regional ocean circulation code must be used. Currently, literature lacks best practices or methodologies as to how ocean velocity data should be used to efficiently identify the highest potential sites in relation to the turbine geometrical features. Even though using 3D CFD software can describe important phenomena such as tip losses [33], wake behavior, interaction with the bathymetry and sea surface, remarkable computational resources would be required for detailed analysis (the computational time of a single 3D CFD analysis is on the order of weeks). Such approach is clearly unfeasible, especially if a site assessment study of a wide area is to be carried out.

In this article, a lower-order but more efficient method able to accomplish a preliminary power assessment analysis is presented. Our model is validated against high-resolution 2D CFD data and then used with dynamic ocean flow data obtained from ocean circulation modeling software to predict the harvestable tidal power in the southern Cape Cod region, prior to environmental impact study.

II. VAWT Model Description

We employ a turbine performance description routine developed at University of Pisa [17] to analytically evaluate the turbine load and power output. The software is based upon the Actuator Disk/Cylinder (AD/C) model [4], based on the Blade Element Momentum (BEM) theory [22], to analytically evaluate momentum sources that simulate the effect of the turbine blades on the flow, obviating the need to model the blades in the computational domain.

Our model can be applied to different VAWT geometries such as Darrieus (straight-bladed) and Troposkien (ϕ-shaped) rotors whose geometric features (e.g. radius R, height H, number of blades N_b, Aspect-Ratio $AR = H/2R$, frontal area $A = 2RH$, etc.) can be freely varied. It is also possible to investigate different airfoil shapes, working conditions (e.g. turbine rotational speed ω, Tip-Speed Ratio $TSR = \omega R/U_\infty$, etc.), nature of flow (e.g. wind, water, etc.).

978-1-5386-4814-8/18/$31.00

A. BEM Momentum Source Computation

The geometric framework employed in our model is thoroughly described by Islam et al. [8]. Let us consider a horizontal sliced plane of a VAWT of height H at an arbitrary vertical position z of thickness Δz as shown in Figure 1. The incoming undisturbed flow velocity, aligned with the x axis, is U_∞ and is slowed down as it approaches the turbine, becoming U_1.

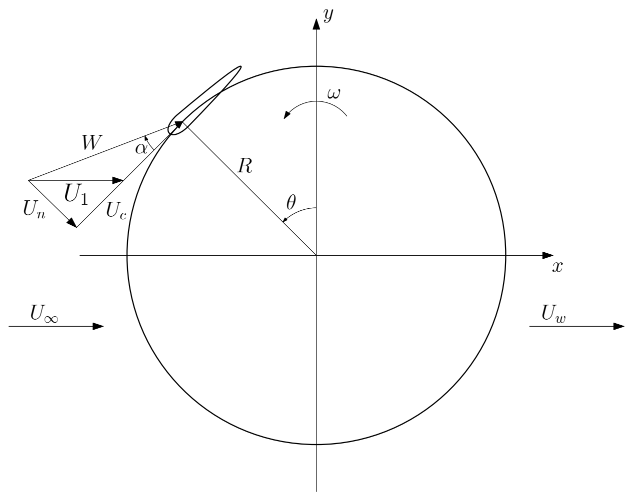

Fig. 1: Geometric framework for BEM analysis.

It follows that

$$U_n(\theta) = U_1 \sin(\theta) \tag{1}$$
$$U_c(\theta) = \omega R + U_1 \cos(\theta) \tag{2}$$
$$W(\theta) = \sqrt{U_c^2(\theta) + U_n^2(\theta)} \tag{3}$$

From which the local geometric angle of attack α and the chord-based Reynolds number Re_c can be evaluated.

$$\alpha(\theta) = \tan^{-1}\left(\frac{U_n(\theta)}{U_c(\theta)}\right) \tag{4}$$
$$Re_c(\theta) = \frac{cW(\theta)}{\nu} \tag{5}$$

It is now possible to evaluate the static aerodynamic coefficients $C_L(\alpha, Re_c)$ and $C_D(\alpha, Re_c)$ from available test data such as Sheldahl et al. [26]. These non-dimensional forces are subsequently projected along the tangential and radial directions, C_T and C_N, and, finally, along directions parallel and perpendicular to the flow, C_X and C_Y respectively.

$$C_T = C_L \sin(\alpha) - C_D \cos(\alpha) \tag{6}$$
$$C_N = C_L \cos(\alpha) + C_D \sin(\alpha) \tag{7}$$
$$C_X = C_T \cos(\theta) - C_N \sin(\theta) \tag{8}$$
$$C_Y = C_T \sin(\theta) + C_N \cos(\theta) \tag{9}$$

The turbine power P and power coefficient C_P can be obtained from the following.

$$P = \frac{N_b}{2\pi} \int_0^{2\pi} \int_0^H \frac{1}{2} \rho c W^2(\theta, k) C_T(\theta, k) \omega R dz d\theta \tag{10}$$
$$C_P = \frac{P}{\frac{1}{2}\rho A U_\infty^3} \tag{11}$$

B. VAWT Unsteady Effects

Compared to HAWTs, VAWTs cannot be considered to work under steady conditions since, during operation, the blades encounter ample and generally fast variation in angle of attack. As a result, unsteady phenomena arise that heavily influence the rotor performance and, therefore, cannot be neglected.

Our code is equipped with sub-models that allow to evaluate the effects of the most important of these phenomena such as dynamic stall, flow curvature and tip losses.

Dynamic stall is characterized by a deviation of aerodynamic data from the static data available in literature. Specifically, under dynamic conditions of time-varying α, an airfoil shows higher peak values of C_L that are obtained for values of α higher than the static stall α. Moreover, there is also a delay in the reattachment of the boundary layer, achieved for α lower than the static stall α. This behavior is due to the fact that, as the angle of attack increases, a vortex of growing intensity is formed near the leading edge of the airfoil (Leading Edge Vortex, LEV), which increases suction on the suction side of the airfoil and delays stall conditions. For very high values of α, the LEV moves towards, and later away from, the trailing edge of the airfoil causing a drop in lift force, sometimes followed by smaller peaks due to secondary vortices. An example of the resulting $C_L(\alpha)$ curve under dynamic conditions is shown in Figure 2. The mathematical details of the model are illustrated in [23] and lead to an adjustment of the C_L and C_D coefficients evaluated in the previous paragraph.

Flow curvature effects are due to the orbital trajectory of the blades which, in turn, induce centrifugal forces on the flow acting on the turbine blades. These phenomena, first analyzed by Migliore et al. [20], lead to an alteration in the dynamics of the boundary layer together with a variation of the local angle of attack along the chord line. Our sub-model is based on the aforementioned work and accounts for this effect by increasing α by a suitable amount, adding a “virtual cambering” to the airfoil.

Finally, the finite aspect ratio of the rotor, which leads to lower aerodynamic performance approaching the tip of the blades, is described via a classic Prandtl tip loss factor [27].

C. Software Working Modes

The software we developed can be used in two different configurations: DMST and Hybrid mode. The former uses the one-dimensional approach proposed by Paraschivoiu [22] and can operate independently of other pieces of software while the latter consists of coupling our code with a CFD solver

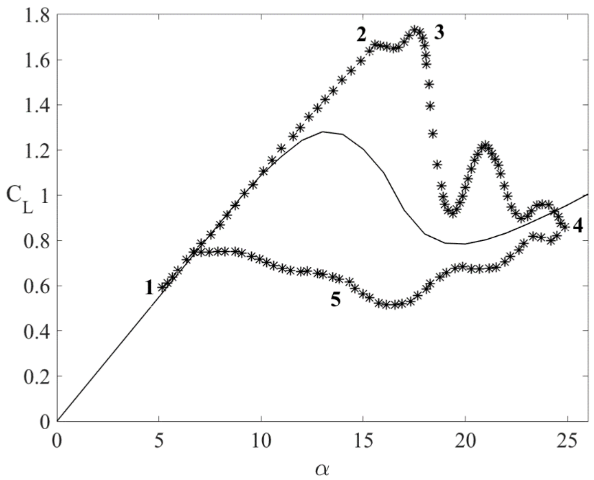

Fig. 2: Example of $C_L(\alpha)$ curve under dynamic conditions ($*$) against static data ($-$) [23].

able to accept external forcing terms in the time-dependent Navier-Stokes momentum equations.

In Hybrid mode, the coupling is achieved by running the sources evaluation routine at the beginning of each timestep using flow data from the previous iteration. The evaluated momentum sources are then passed to the CFD solver for the time-stepping phase and applied to the computational domain. In this configuration, our code has been coupled with the CFD solver ANSYS Fluent via the integrated User-Defined Function (UDF) feature. A more in-depth explanation of this working configuration can be found in [24]. This kind of approach has recently appeared in literature [25, 1, 2].

In DMST mode, a simplified approach is adopted in order to obtain a quick and fairly accurate performance prediction of the rotor in steady conditions, without the need for a computational mesh for the entire physical domain. This is accomplished by dividing the turbine domain into a series of streamtubes parallel to the flow direction, each split into two linked upstream and downstream halves (Figure 3), through which an inviscid, steady, one dimensional flow is assumed. For each half streamtube, mass, momentum and energy balances are solved in their integral form.

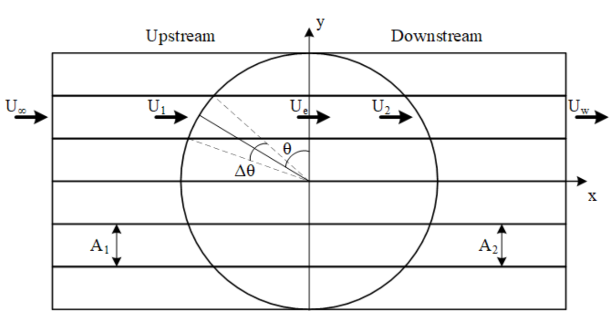

Fig. 3: Example of DMST scheme.

Let us consider a single streamtube at the azimuthal position θ of infinitesimal $\Delta\theta$ width and area A_i, where the subscript 1 designates the upstream half and 2 the downstream one. The balance equations become the following.

$$A_i = R\Delta\theta\,|\sin(\theta)| \tag{12}$$

$$\dot{m} = \rho U_1 A_1 = \rho U_2 A_2 \tag{13}$$

$$\dot{m}\,(U_\infty - U_e) = F_{1,x} \tag{14a}$$

$$\dot{m}\,(U_e - U_w) = F_{2,x} \tag{14b}$$

$$\frac{1}{2}\dot{m}\left(U_\infty^2 - U_e^2\right) = F_{1,x}U_1 \tag{15a}$$

$$\frac{1}{2}\dot{m}\left(U_e^2 - U_w^2\right) = F_{2,x}U_2 \tag{15b}$$

As reported by [22], due to the 1D nature of this model, the mass balance is not respected since $A_1 = A_2$ is assumed but this is not considered to be a large source of error. Defining the induction factors for both halves of the streamtube, $a_1 = U_1/U_\infty$ and $a_2 = U_2/U_e$, and combining the previous equations

$$U_e = U_\infty(2a_1 - 1) \tag{16}$$

$$U_w = U_e(2a_2 - 1) \tag{17}$$

$$U_2 = U_\infty(2a_1 - 1)a_2 \tag{18}$$

Knowing U_1 and U_2, it is possible to evaluate the thrust force coefficient C_X of one blade element acting on the streamtube via equations (1) to (8). The total thrust force F_X is

$$F_X = \frac{1}{2}\rho c W^2 C_X \left(\frac{N_b\Delta\theta}{2\pi}\right) \tag{19}$$

Where the bracketed term is added to consider a time-averaging over one revolution period in the single streamtube.

The total thrust force F_X can be also obtained from the thrust force coefficient definition.

$$C_{X,1} = \frac{F_X}{\frac{1}{2}\rho A_1 U_\infty^2} \tag{20a}$$

$$C_{X,2} = \frac{F_X}{\frac{1}{2}\rho A_2 U_e^2} \tag{20b}$$

Equations (12) to (18) and (20) can be used to prove that

$$C_{X,i} = 4a_i(1 - a_i) \quad for\ i = 1, 2 \tag{21}$$

However, this theoretical result shows little agreement with experimental data for $a_i < 0.6$. Therefore, the following empirical correlation, appropriately reversed, by Spera [28] has been used.

$$1 - a_i = 0.27C_{X,i} + 0.1C_{X,i}^3 \quad for\ i = 1, 2 \tag{22}$$

It is now possible to iteratively evaluate a_i for each half streamtube so that F_X obtained via equation (19) and equation (20) match. Due to the linking of the streamtube halves, it is necessary to solve the upstream part of the turbine first.

This computational algorithm has been implemented in an in-house *MATLAB* routine in which the turbine is discretized in an arbitrary number of horizontal streamtubes $n_{ring} = 2\pi/\Delta\theta$ and vertical planes $n_z = H/\Delta z$. The sub-models mentioned in paragraph II-B have been implemented together with a sub-routine which allows a better description of the diverging streamlines direction in the upwind part of the rotor. In order to simulate the unsteady conditions needed for the dynamic stall sub-routine, the DMST is run iteratively, simulating a time-stepping in which the blades are supposed to advance through the azimuthal direction by one $\Delta\theta$ each time-step. The time-stepping is carried out until the turbine power coefficient C_P relative variation between time-steps becomes negligible.

III. Model Validation

Our turbine performance prediction routine has been validated against high-resolution CFD simulations. The Hybrid mode validation and sensitivity analysis have been carried out in [24] and showed that satisfactory matching with reference data is reached with a reduction in computational time required by a factor 10. Therefore, only the validation of the DMST configuration will be carried out in this work.

A. DMST Validation Computational Setup

The DMST configuration has been validated by investigating the performance of a straight-bladed water turbine that feature a radius $R = 3.16228\ m$, a chord $c = 0.42162\ m$ and a number of blades $N_b = 4$. The solidity of the turbine is $\sigma = N_b c/2\pi R = 8.5\%$. The turbine is subject to an incoming flow of $U_\infty = 1.75\ m/s$ and its performance is analyzed for varying TSR.

Reference data has been obtained from a series of 2D CFD simulations run with the software ANSYS Fluent v15.0. To simulate the turbine rotation two different structured multi-block grids are used: a fixed sub-grid with the external dimensions of the flow domain and a rotating sub-grid that includes the VAWT geometry. The latter possesses a relative motion with respect to the former grid by means of the sliding mesh technique. The dimensions of the fixed grid were set large enough to avoid any blockage effect on the turbine($60D$ in the crosswise and in the streamwise directions). Turbulence was modeled with the $k - \omega$ SST (Shear Stress Transport) model [19, 30] widely used in the simulation of wind or tidal vertical axis rotors, since it is well suited for flows with strong adverse pressure gradient as those involved in VAWTs, especially when operating at low TSRs. In order to correctly describe the boundary layer on the blade, the wall distance from the first layer of cells was set to keep $y+$ low enough (< 0.5) to capture flow separation phenomena [18]. The velocity-pressure coupling algorithm was SIMPLEC (Semi-Implicit Method for Pressure Linked Equations-Consistent). The spatial discretization was set to Green-Gauss node-based for gradient. econd order schemes were adopted for pressure, momentum, turbulent kinetic energy and specific dissipation rate formulations. A second order implicit scheme was also used for temporal discretization.

To better assess the quality of the prediction of the DMST configuration, simulations in Hybrid mode have also been run for the same test case. Identical solver settings used in 2D CFD simulations have been employed while the computational grid needed slight modifications. Specifically, while the outer fixed sub-grid remained unchanged, the internal one was modified so that the rotating blades were substituted by a non-rotating circular ring of 96 cells where the evaluated momentum sources have been applied.

Due to the absence of a computational grid in DMST models, the setup of our DMST routine consists only in choosing the variable n_{ring}, i.e. the total number of upstream and downstream streamtubes. Sensitivity analysis on the DMST routine showed that no meaningful variation of results is obtained for $n_{ring} > 40$, therefore, such a value has been chosen for all the simulations in this work.

B. Results

Figure 4a shows the turbine one-blade power coefficient C_P as a function of the azimuthal position θ for $TSR = 2.5$, which is the optimal one according 2D CFD simulations. The plot shows a remarkably good agreement between our model in both working configurations and the 2D CFD results. The DMST and Hybrid modes are able to correctly reproduce the $C_P(\theta)$ curve in the range $[0° - 90°]$, including the peak, while small under-estimation can be seen in the DMST curve for the rest of the upstream section. In the downstream half of the turbine, all the curves show two smaller peaks whose intensities, however, are overestimated by the DMST routine. Such results are likely due to the fact that the DMST code does not account for streamtube expansion in the downstream half of the rotor. Indeed, expansion due to mass conservation would cause a distortion and slowdown of the flow that would lead to lower angles of attack in the downstream half on the turbine, lowering the power output [22]. This problem does not arise in Hybrid mode since mass and momentum balances are handled by the CFD solver and do not require further modeling.

Figure 4b illustrates the total turbine C_P with varying TSR. The qualitative trend of the 2D CFD curve is matched by both configurations even though the Hybrid one correctly predicts the highest C_P for $TSR = 2.5$ whereas the DMST one slightly anticipates it at $TSR = 2.35$. Values of C_P assessed by the DMST and Hybrid routines tend to be slightly higher compared to the 2D CFD ones, with this difference increasing for TSR away from the optimal value of 2.5, where the highest relative difference in performance between DMST and 2D CFD amounts to less than 7%. Such overestimation was expected, given the simplified approach inherent to the DMST modeling. For lower values of TSR, the DMST mode achieves the most overestimation while, for higher ones, the Hybrid configuration predicts the highest C_P.

Finally, it must be pointed out that the computational resources needed by the code are limited, especially in DMST mode. In fact, DMST reached convergence in a time in the order of minutes, Hybrid mode in the order of hours while 2D CFD simulations required a time on the scale of days.

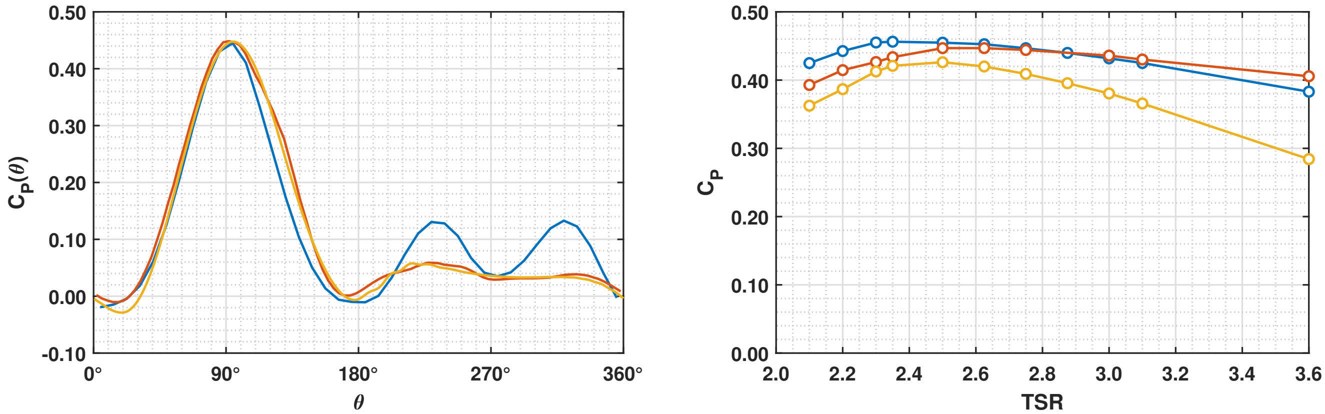

(a) One-blade $C_P(\theta)$ for $TSR = 2.5$.

(b) Total turbine C_P as a function of TSR.

Fig. 4: Performance comparison between DMST model (blue), Hybrid model (red) and 2D CFD (orange) simulations.

IV. Practical Application: Cape Cod Region Power Assessment

As a practical application of our DMST routine, an assessment of the power available for harvesting via Vertical Axis Water Turbines has been carried out using realistic ocean flow data derived from CFD simulations [7, 6]. The investigated region is the southern shore of Cape Cod, MA, specifically the area extending between $40°30'6''N$ and $41°44'53''N$ and between $70°6'36''W$ and $69°7'33''W$. This area has been chosen for its acknowledged high tidal potential for both short and long-term applications [9] which also led, for example, to the creation of a tidal turbine test site near Bourne, MA [3]. It was decided to employ the same straight-bladed turbine illustrated in Section II with an Aspect-Ratio AR of 1.35. However, it must be pointed out that this tool can also be used to optimize the geometry of the rotor for maximum power extraction. Such turbine is supposed to work at $TSR = 2.5$, which was found to be the optimal one in Section III, and to be placed on a floating platform so that the vertical rotational axis is perpendicular to the free surface of the sea. In order to reduce the influence of 3D flow phenomena which the DMST model would not be able to capture, a clearance of 2 m is allowed both over and under the turbine blades.

A. Methodology

The ocean flow data has been obtained from simulations run with the PE CFD code based on the work by Haley et al. [7, 6] and developed by the MSEAS group of Massachusetts Institute of Technology. The PE software is able to model multiscale ocean dynamics governed by primitive equations (PEs) over the tidal scales of our interest, also accounting for complex bathymetry.

Outputs of the PE software include depth-varying scalar quantities like temperature and salinity, and vector quantities such as zonal $u(z)$ and meridional velocity $v(z)$. Examples of recent applications are reviewed in [14, 16, 5, 11, 21].

The computational domain analyzed in the current work is presented in Figure 5. The spatial and temporal resolution are 600 m and 1 hour respectively.

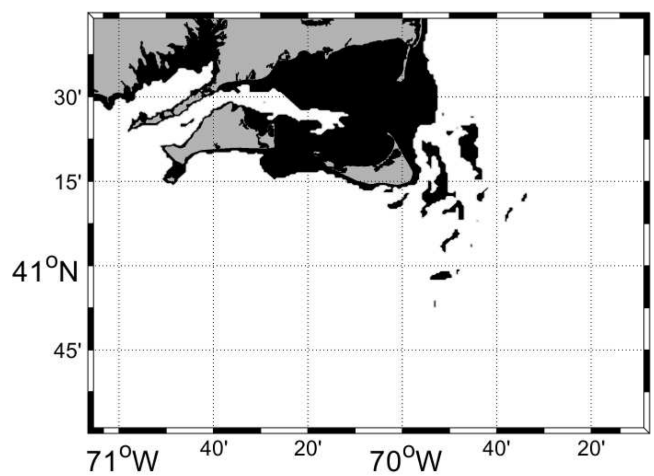

Fig. 5: Site assessment computational domain. Gray areas are land and black areas are locations where turbine clearance is not achieved.

Tidal-period-averaged velocity data in the above-mentioned region simulated between August 13 2017 and August 18 2017 (Figure 6) have been used as inputs for the DMST routine. Since the velocity profile varies along the z-direction, the turbine has been discretized in n_z horizontal planes, each of which is invested by an undisturbed velocity $U_\infty(z)$ and solved independently of the others due to the 2D nature of DMST model.

The mean undisturbed velocity U_{3D}, mean turbine Tip-Speed Ratio TSR_{3D}, total power P_{3D} and power coefficient $C_{P_{3D}}$ of the rotor become:

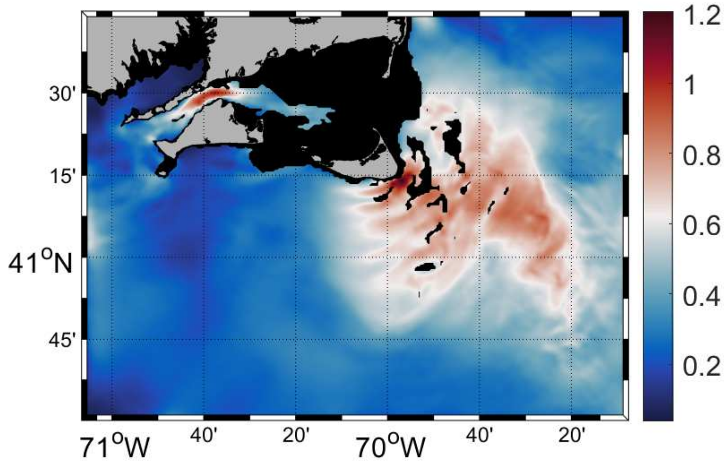

(a) Tidal-period-averaged and z-averaged U_∞ (m/s).

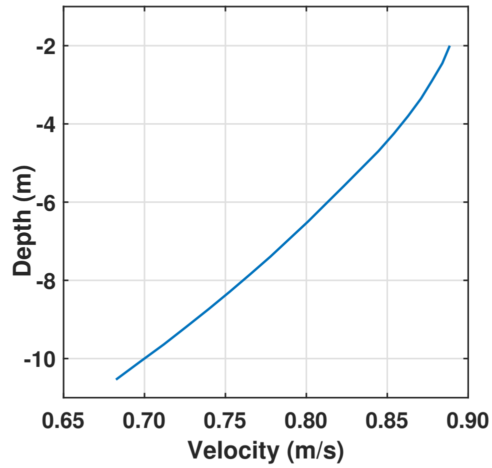

(b) Example of $U_\infty(z)$.

Fig. 6: Ocean flow velocity data over computational domain.

$$U_{3D} = \frac{\sum_{n_z} U_\infty(z)}{n_z} \tag{23}$$

$$TSR_{3D} = \frac{\omega R}{U_{3D}} \tag{24}$$

$$P_{3D} = \sum_{n_z} P(z) \tag{25}$$

$$C_{P_{3D}} = \frac{P_{3D}}{\frac{1}{2}\rho A U_{3D}^3} \tag{26}$$

The DMST evaluation has been run on a sub-sampled grid along the x and y directions obtained from the original computational domain and a linear interpolation has been carried out in the intermediate points. The simulation has not been run on grid points where turbine clearance is not achieved.

B. Results

The results of the analysis are presented in Figure 7. Figure 7a shows that values of $C_P > 0.35$ are reached in most of the investigated area with highest peaks found in the Vineyard Sound strait, between Martha's Vineyard and Naushon Island, and slightly away from the south-eastern shoreline of Nantucket Island, towards the open Atlantic Ocean. Lower values are concentrated along south-western borders of the computational domain. Low values of C_P are due to the turbine planes not working under ideal TSR conditions, i.e. the more turbine planes have $TSR(z) = \omega R / U_\infty(z)$ different from TSR_{3D}, the less efficient the rotor is. Such scenarios arises when highly z-varying velocity profiles flow through the turbine.

However, a marine site can be deemed interesting from a tidal energy extraction point of view not only if energy can be extracted efficiently, i.e., with a high C_P, but also if the power output is sufficiently high. Figure 7b shows the power distribution of the investigated area. Two clear areas of tidal interest can be identified with an estimated turbine power output of around $10\ kW$. It is interesting to note that these locations match the previously highlighted high-C_P areas. Therefore, these sites become clear candidates for further, higher-order simulations (Hybrid mode, 3D CFD, etc.) to be run in order to obtain a better description of the rotor power harvesting capabilities.

Of course, in addition to tidal power, sustainable energy extraction demands careful forecasting and assessment of environmental impacts and risks in accord with uncertainties [13, 15].

V. Conclusions

A routine for the prediction of the power harvested by Vertical Axis Water Turbines (VAWTs) is presented. Our code is able to function in two configurations: Hybrid mode, i.e. in tandem with a CFD software, and DMST mode, i.e. stand-alone by employing the DMST theory. The latter can be used as the first step in a site assessment analysis to quickly identify small regions of interest of high power harvesting potential where further higher-order analyses can be carried out. Despite the mismatch for lower and higher TSR than the optimal one, our DMST model only slightly overestimates the power production under ideal working conditions. As a consequence, even if more work must be done to improve the subroutines and account for phenomena such as streamtubes expansion, our code can be used in its current state for practical applications with good results. The ultimate goal of our research groups is to create a fast, valuable and comprehensive, i.e. progressively higher-order and more accurate, tool for turbine farms planning and also to model and account for environmental risks and impacts, so as to ensure sustainable ocean utilization and conservation.

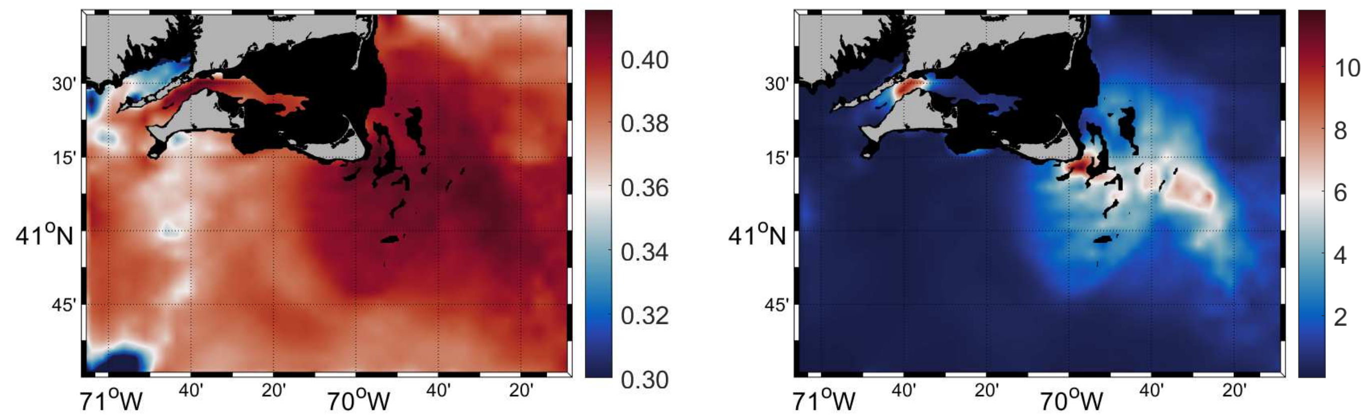

(a) Turbine $C_{P_{3D}}$ (non-dimensional) over computational domain.

(b) Turbine P_{3D} (kW) over computational domain.

Fig. 7: Results of site assessment analysis using the DMST routine.

ACKNOWLEDGMENT

We thank the MSEAS group at MIT for insightful discussions. We are grateful to the MIT International Science and Technology Initiatives (MISTI) – University of Pisa (MIT-UNIPI) program for seed support that allowed us to kick-start this collaborative project. The MSEAS group also thanks the National Science Foundation for support under grant EAR-1520825 (Hazards SEES – ALPHA), the Office of Naval Research for support under grant N00014-14-1-0725 (Bays-DA), and the National Oceanographic Partnership Program (NOPP) for support under grant N00014-15-1-2597 (Seamless Multiscale Forecasting), each to the Massachusetts Institute of Technology. S.D. thanks Stefano Letizia for insightful discussions.

REFERENCES

[1] M. Abkar and J. O. Dabiri. Self-similarity and flow characteristics of vertical-axis wind turbine wakes: an LES study. *Journal of Turbulence*, 18(4):373–389, 2017.

[2] P. Bachant, A. Goude, and M. Wosnik. Actuator line modeling of vertical-axis turbines. may 2016.

[3] S.B. Barrett, M.L. Merrill, and J.R. Miller. Bourne tidal test site: BTTS now ready for partial-scale device testing. *Sea Technology*, 59(4):10–13, 2018.

[4] T. Burton, N. Jenkins, D. Sharpe, and E. Bossanyi. *Wind Energy Handbook Second Edition*. 2011.

[5] J. Coulin, P. J. Haley, Jr., S. Jana, C. S. Kulkarni, P. F. J. Lermusiaux, and T. Peacock. Environmental ocean and plume modeling for deep sea mining in the bismarck sea. In *Oceans 2017 - Anchorage*, Anchorage, AK, September 2017.

[6] P. J. Haley, Jr., A. Agarwal, and P. F. J. Lermusiaux. Optimizing velocities and transports for complex coastal regions and archipelagos. *Ocean Modeling*, 89:1–28, 2015.

[7] P. J. Haley, Jr. and P. F. J. Lermusiaux. Multiscale two-way embedding schemes for free-surface primitive equations in the "multidisciplinary simulation, estimation and assimilation system". *Ocean Dynamics*, 60(6):1497–1537, 2010.

[8] M. Islam, D. S. K. Ting, and A. Fartaj. Aerodynamic models for Darrieus-type straight-bladed vertical axis wind turbines. *Renewable and Sustainable Energy Reviews*, 12(4):1087–1109, 2008.

[9] L. Kilcher, R. Thresher, and H. Tinnesand. Marine Hydrokinetic Energy Site Identification and Ranking Methodology Part II: Tidal Energy. Technical Report October, National Renewable Energy Laboratory (NREL), Golden, CO (United States), oct 2016.

[10] M. Kinzel, Q. Mulligan, and J. O. Dabiri. Energy exchange in an array of vertical-axis wind turbines. *Journal of Turbulence*, 13:N38, jan 2012.

[11] C. S. Kulkarni, P. J. Haley, Jr., P. F. J. Lermusiaux, A. Dutt, A. Gupta, C. Mirabito, D. N. Subramani, S. Jana, W. H. Ali, T. Peacock, C. M. Royo, A. Rzeznik, and R. Supekar. Real-time sediment plume modeling in the Southern California Bight. In *OCEANS Conference 2018*, Charleston, SC, October 2018. IEEE. In press.

[12] N. D. Laws and B. P. Epps. Hydrokinetic energy conversion: Technology, research, and outlook. *Renewable and Sustainable Energy Reviews*, 57:1245–1259, may 2016.

[13] P. F. J. Lermusiaux, C.-S. Chiu, G. G. Gawarkiewicz, P. Abbot, A. R. Robinson, R. N. Miller, P. J. Haley, Jr, W. G. Leslie, S. J. Majumdar, A. Pang, and F. Lekien. Quantifying uncertainties in ocean predictions. *Oceanography*, 19(1):92–105, 2006.

[14] P. F. J. Lermusiaux, P. J. Haley, Jr., S. Jana, A. Gupta, C. S. Kulkarni, C. Mirabito, W. H. Ali, D. N. Subramani, A. Dutt, J. Lin, A. Shcherbina, C. Lee, and A. Gangopadhyay. Optimal planning and sampling predictions for autonomous and lagrangian platforms and sensors in the

northern Arabian Sea. *Oceanography*, 30(2):172–185, June 2017. Special issue on Autonomous and Lagrangian Platforms and Sensors (ALPS).

[15] P. F. J Lermusiaux, P. J. Haley, Jr, and N. K. Yilmaz. Environmental prediction, path planning and adaptive sampling: sensing and modeling for efficient ocean monitoring, management and pollution control. *Sea Technology*, 48(9):35–38, 2007.

[16] P. F. J. Lermusiaux, D. N. Subramani, J. Lin, C. S. Kulkarni, A. Gupta, A. Dutt, T. Lolla, P. J. Haley, Jr., W. H. Ali, C. Mirabito, and S. Jana. A future for intelligent autonomous ocean observing systems. *Journal of Marine Research*, 75(6):765–813, November 2017. The Sea. Volume 17, The Science of Ocean Prediction, Part 2.

[17] S. Letizia and S. Zanforlin. Hybrid CFD-source Terms Modelling of a Diffuser-augmented Vertical Axis Wind Turbine. *Energy Procedia*, 101(November):1280–1287, 2016.

[18] T. Maître, E. Amet, and C. Pellone. Modeling of the flow in a Darrieus water turbine: Wall grid refinement analysis and comparison with experiments. *Renewable Energy*, 51:497–512, mar 2013.

[19] F. R. Menter. Two-equation eddy-viscosity turbulence models for engineering applications. *AIAA Journal*, 32(8):1598–1605, aug 1994.

[20] P. G. Migliore, W. P. Wolfe, and J. B. Fanucci. Flow Curvature Effects on Darrieus Turbine Blade Aerodynamics. *Journal of Energy*, 4(2):49–55, mar 1980.

[21] C. Mirabito, D. N. Subramani, T. Lolla, P. J. Haley, Jr., A. Jain, P. F. J. Lermusiaux, C. Li, D. K. P. Yue, Y. Liu, F. S. Hover, N. Pulsone, J. Edwards, K. E. Railey, and G. Shaw. Autonomy for surface ship interception. In *Oceans '17 MTS/IEEE Conference*, Aberdeen, June 2017.

[22] I. Paraschivoiu. *Wind Turbine Design with Emphasis on Darrieus Concept*. 2002.

[23] B. Rocchio, C. Chicchiero, M. V. Salvetti, and S. Zanforlin. Towards a general dynamic stall model. In *AIDAA XXIV International Conference*, 2017.

[24] B. Rocchio, S. Deluca, M. V. Salvetti, and S. Zanforlin. Development of a BEM-CFD tool for Vertical Axis Wind Turbines based on the Actuator Disk model. In *73rd Conference of the Italian Thermal Machines Engineering Association (ATI 2018)*, Pisa, 2018. In Press.

[25] S. Shamsoddin and F. Porté-Agel. A Large-Eddy Simulation Study of Vertical Axis Wind Turbine Wakes in the Atmospheric Boundary Layer. *Energies*, 9(5):366, may 2016.

[26] R. E. Sheldahl and P. C. Klimas. Aerodynamic characteristics of seven symmetrical airfoil sections through 180-degree angle of attack for use in aerodynamic analysis of vertical axis wind turbines. Technical report, Sandia National Laboratories (SNL), Albuquerque, NM, and Livermore, CA (United States), mar 1981.

[27] W. Z. Shen, R. Mikkelsen, J. N. Sørensen, and C. Bak. Tip loss corrections for wind turbine computations. *Wind Energy*, 8(4):457–475, 2005.

[28] D. A. Spera. Wind Turbine Technology: Fundamental Concepts of Wind Turbine Engineering. *Solar Energy*, 62(2):XVII, 2009.

[29] A. Vergaerde, T. De Troyer, J. Kluczewska-Bordier, N. Parneix, F. Silvert, and M. C. Runacres. Wind tunnel experiments of a pair of interacting vertical-axis wind turbines. *Journal of Physics: Conference Series*, 1037:072049, jun 2018.

[30] D. C. Wilcox. Formulation of the k-w Turbulence Model Revisited. *AIAA Journal*, 46(11):2823–2838, nov 2008.

[31] S. Zanforlin. Advantages of vertical axis tidal turbines set in close proximity: A comparative CFD investigation in the English Channel. *Ocean Engineering*, 156:358–372, may 2018.

[32] S. Zanforlin, F. Burchi, and N. Bitossi. Hydrodynamic Interactions Between Three Closely-spaced Vertical Axis Tidal Turbines. *Energy Procedia*, 101:520–527, nov 2016.

[33] S. Zanforlin and S. Deluca. Effects of the Reynolds number and the tip losses on the optimal aspect ratio of straight-bladed Vertical Axis Wind Turbines. *Energy*, 148:179–195, apr 2018.